A Novel Approach for Monodisperse Samarium Orthovanadate Nanocrystals: Controlled Synthesis and Characterization

Thanh-Dinh Nguyen,[†] Cao-Thang Dinh,[†] Dinh-Tuyen Nguyen,[‡] and Trong-On Do*,[†]

Department of Chemical Engineering, Laval University, Quebec G1K 7P4 Canada, Institute of Chemistry, Vietnamese Academy of Science and Technology

Received: July 27, 2009; Revised Manuscript Received: September 5, 2009

A new solvothermal approach has been developed for the synthesis of monodisperse and well-crystallized $SmVO_4$ nanocrystals with different morphologies from the reaction of $Sm(OA)_3$ and $VO_4(TOA)_3$ complexes in toluene in the presence of surfactant (oleylamine or oleic acid) through a solvothermal pathway. The present solvothermal approach is simple and reproducible and employs a relatively mild reaction temperature. The obtained $SmVO_4$ nanocrystals were characterized by means of transmission electron microscopy, selected area electronic diffraction (SAED), X-ray diffraction (XRD), Elemental dispersive spectrum, X-ray photoelectron spectra (XPS), UV−visible, thermogravimetric differential thermal analysis TGA−DTA, FTIR, and N_2 adsorption/desorption isotherms (BET) techniques. The SAED and XRD patterns confirmed that the structure of the synthized $SmVO_4$ nanocrystals is single-crystalline tetragonal. The size, shape, and aspect ratio of products can be readily controlled by adjusting the reaction parameters, such as the nature and amount of surfactant, and the concentration of the metal complex precursors. The $SmVO_4$ nanocrystals with spherical and hexagonal shapes were obtained by using oleylamine or oleic acid as a nonselective and selective surfactant, respectively, under the same synthesis conditions. Furthermore, the average particle size is tunable from 30 to 3 nm by increasing the oleylamine concentration from 0.025 to 0.43 M in the synthesis solution. The shape evolution from nanocores to nanowires can also be obtained by increasing the metal complex precursor concentration; it is associated with the increase in the chemical potential in the reaction solution. The XPS results revealed only one oxidation state for Sm^{3+} and V^{5+} on the $SmVO_4$ nanocrystal surface, even after calcinations compared two oxidation states (e.g., Sm^{2+}/Sm^{3+} and V^{4+}/V^{5+}) of the single samarium oxide and vanadium oxide NPs, respectively. Our synthetic approach can be further extended to the synthesis of other uniform rare earth orthovanadate, molybdate, and tungstate nanocrystals.

Downloaded by UNIV LAVAL on October 22, 2009 | http://pubs.acs.org
Publication Date (Web): October 6, 2009 | doi: 10.1021/jp907129t

1. Introduction

The synthesis of mixed metal oxide nanocrystals (NCs) composed of two or more different components has attracted particular interest due to the possibility of the mergence of material properties together, which is not usually attainable in single-component nanocrystals.[1−3] Monodisperse mixed oxide nanocrystals with small dimensions are often referred to as "artificial atoms" with novel properties because of their atomic-like behaviors which are not achieved by their bulk counterparts.[4,5] The synthesis of monodisperse mixed oxide nanocrystals with controllable morphologies is, thus, a key goal in modern materials chemistry and has attracted rapidly growing interest in recent years.[6−10] Furthermore, because of size- and shape-dependent properties of nanocrystals, a precise control over size and shape can lead to the formation of materials with unique physical and chemical properties.[11−13] For example, zero- and one-dimensional (0D/1D) nanostructures such as nanospheres and nanowires show great promise in many applications.[14−16] In the bottom-up syntheses, the sterically diffusive kinetics and selective binding or nonbinding of surfactant molecules to different faces of the growing nanocrystal can also control the product's morphology due to the possibility of breaking the limitations of crystal growth dynamically.[17−21] In some cases, the formation of the intrinsic anisotropic nanocrystals is found to be a highly kinetics-driven process, which occurs far away from the thermodynamic equilibrium, and must be overdriven by high precursor monomer concentrations.[22]

$SmVO_4$ nanocrystals have been extensively studied as a promising material in recent years because they exhibit unique properties and applications in many fields, such as catalysis,[23] gas sensors,[24] optical polarizers,[25] lithium intercalated electrodes,[26] thin film phosphors,[27] laser host materials,[28] solar cells,[29] and unusual magnetic materials.[30] For example, these $SmVO_4$ nanocrystals exhibit high activity and selectivity as catalysts for many organic reactions, such as oxidative dehydrogenation of alkanes, olefins, ethylbenzene and oxidation of hydrogen sulfide to elemental sulfur.[31−35] Their high catalytic activity has been correlated to the redox cycle between V^{5+} and V^{4+} in the $SmVO_4$ crystal lattice and cation vacancies sites, which occurs during oxidative dehydrogenation.[35,36] The unstable surface-active sites are oxygen vacancies associated with V^{4+} ions. The activation of oxygen species generating the adsorbed O_2 or O^- takes place on the V^{4+} sites. The oxidation selectivity of the rare earth orthovanadates ($REVO_4$) is higher than that of vanadia and might be due to the greater difficulty in removing a lattice oxygen from the RE-O−V bond in $REVO_4$ than from the V−O−V bond in V_2O_5.[37] The dehydrogenation yield of $SmVO_4$ is much better than that of the corresponding single oxide catalysts (e.g., vanadia and samaria), which might be a result of the reducibility difference between vanadium and

* To whom correspondence should be addressed. E-mail: Trong-On.Do@gch.ulaval.ca.
[†] Laval University.
[‡] Vietnamese Academy of Science and Technology.

10.1021/jp907129t CCC: $40.75 © 2009 American Chemical Society
Published on Web 10/06/2009

samarium cations.[38] Consequently, oxygens in the $SmVO_4$ lattice are less labile than those of both vanadia and samaria.[38] Furthermore, numerous studies have demonstrated that not only particle size and shape but also chemical composition play key roles in defining activity and selectivity in the catalytic processes.[39−41]

To date, most of the strategies for the synthesis of $SmVO_4$ nanocrystals have been focused on solid-state reaction and hydrothermal methods. The conventional solid-state reaction was used for the synthesis of these materials by heating the constituent bulk single metal oxide powders in a stoichiometric ratio at relatively high temperature. For example, Saito et al.[42] synthesized $SmVO_4$ crystals by heating at 1000−1100 °C after mechanically milling the mixture of single oxides of Sm_2O_3 and V_2O_5 powders. Nevertheless, this route was hard to control over the kinetics of nucleation−growth process, often giving particle agglomeration, low chemical homogeneity, and poor crystallinity. The solution-based route, in contrast, was considered as one of the most convenient methods for the controlled synthesis of $SmVO_4$ nanocrystals. For example, Sun et al.[43] reported that $SmVO_4$ nanorods can be formed in the absence of surfactant or template agents using inorganic salts as raw materials. Ramanan et al.[44] had also directly precipitated these salts for the formation of the flake-shaped $SmVO_4$ microcrystals. The synthesis of regular square $SmVO_4$ nanocrystals from the reaction of samarium nitrates and ammonium vanadates in water/ethanol/oleic acid system was recently published by Li group.[45] Despite these exciting developments, the precise size and shape manipulation of uniform $SmVO_4$ nanocrystals, particularly spherical- and wire-like morphologies, as well as the investigation of their oxidation states have not been reported so far.

It can thus be expected that developing a low cost and convenient method for the synthesis of monodisperse $SmVO_4$ nanocrystals with controlled, well-defined sizes, shapes, and structure opens enormous possibilities for engineering catalysts with enhanced activity and selectivity.[46,47] For this purpose, the solvothermal method is widely accepted as a valuable process used for the preparation of such materials with well-controlled morphology, crystal growth orientation, and structural properties due to the kinetic equilibrium between dissolution and decomposition of the precursors in organic media at relatively mild reaction temperatures.[48−50] Recently, our group has developed a solvothermal approach for the shape-selective synthesis of vanadium oxide nanocrystals through the decomposition of vanadium diperoxotetraalkylammonium complexes in a toluene/aliphatic amine system. It was found that the desired size and shape can be controlled by different synthesis parameters, such as steric ligands of complexes, alkyl chain lengths of capping agents, and the nature of the solvent.[51]

In this present study, we report a new approach for the controllable synthesis of monodisperse and well-crystallized $SmVO_4$ mixed oxide nanocrystals with different shapes, such as spherical, hexagonal, core, and wire, from the reaction of $Sm(OA)_3$ and $VO_4(TOA)_3$ complexes in toluene in the presence of surfactant (oleylamine or oleic acid) through a solvothermal pathway. $Sm(OA)_3$ and $VO_4(TOA)_3$ complex precursors were presynthesized from the reaction of the inorganic sources and organic ligands. The obtained nanocrystals are highly dispersible in nonpolar organic solvents. The effect of the nature and amount of surfactant as well as metal complex precursor concentration on size and shape of the resulting $SmVO_4$ nanocrystals is studied. The possible mechanism for the formation of the nanocrystals with various sizes and shapes is also proposed.

2. Experimental Section

Starting Materials. All chemicals were used as received without further purification. Samarium nitrate hexahydrate ($Sm(NO_3)_3 \cdot 6H_2O$, 99.9%), vanadium pentaoxide (V_2O_5, 99.6%), tetraoctylammonium bromide ($[CH_3(CH_2)_7]_4NBr$ or TOABr, ≥98%), potassium oleate ($C_{17}H_{34}COOK$ or KOA 40 wt % paste in water), oleylamine ($C_{18}H_{35}NH_2$ or OM, technical grade, 70%), oleic acid ($C_{18}H_{35}COOH$ or OA, technical grade, 90%), were purchased from Sigma-Aldrich. Sodium hydroxide (NaOH, 97.0%) and all solvents used, such as toluene and ethanol, were of analytical grade and purchased from Reagent ACS.

Synthesis of $SmVO_4$ Nanocrystals. ***Preparation of $Sm(OA)_3$ Complexes.*** To prepare rare earth oleate complexes, an organic solution was produced from adding 40 mL of toluene into the ethanol solution (10 mL) containing potassium oleate (KOA, 6.4−24.8 g or 0.008−0.031 mol). The organic solution was added to 30 mL of a $Sm(NO_3)_3 \cdot 6H_2O$ aqueous solution (0.086−0.346 M) with a Sm^{3+}/OA^- molar ratio of 1:3 and then transferred to a flask. The two-phase mixture was heated to 70 °C for 60 min with vigorous stirring, and the organic solution became light yellow after being reacted, indicating the occurrence of the coordinated reaction of Sm^{3+} and OA^- for the complex formation. Subsequently, the upper deep-orange supernatant toluene solution (40 mL) containing $Sm(OA)_3$ complexes (0.065−0.260 M) was isolated.

Preparation of $VO_4(TOA)_3$ Complexes. Commercial bulk V_2O_5 powder (0.24−0.96 g (0.0013−0.0052 mol)) of was dissolved in 20 mL of an aqueous NaOH solution and vigorously stirred at room temperature for 30 min. V_2O_5 powders were completely dissolved in the dilute NaOH solution to give a homogeneous, light orange Na_3VO_4 aqueous solution (0.133−0.520 M). Then 40 mL of toluene solution (0.040−0.159 M) containing a cationic phase-transfer reagent ($[CH_3(CH_2)_7]_4NBr$ or TOABr, 0.87−3.48 g) was added to the above solution, and the VO_4^{3-}/TOA^+ molar ratio was close to 1:3. The two-phase mixture was vigorously stirred at room temperature. After 30 min, VO_4^{3-} anions in the aqueous phase were completely extracted into the toluene phase, and a light orange toluene solution was observed. Subsequently, the upper light orange supernatant toluene solution (40 mL) containing $VO_4(TOA)_3$ complexes (0.065−0.260 M) was isolated.

Synthesis of $SmVO_4$ Nanocrystals. Typically, the two above toluene solutions containing the $Sm(OA)_3$ and $VO_4(TOA)_3$ complexes (0.065−0.260 M) were mixed together at a Sm/V molar ratio of 1:1, and 1−20 mL of oleylamine (OM) or oleic acid (OA) (0.025−0.43 M) was added under stirring. The reaction solution was transferred into a 140-mL Teflon-lined stainless steel autoclave and was heated at 180 °C for 16 h in an oven. After the reaction, the autoclave was cooled in tap water, and the obtained products were easily precipitated by excess ethanol and redispersed preferably in nonpolar solvents (e.g., toluene, hexane, etc.). The precipitation−redispersion process was repeated several times to purify the produced $SmVO_4$ nanocrystals. The different reaction conditions, such as the nature and amount of surfactant and the metal complex precursor concentration, were tested to control the sizes and the shapes of the $SmVO_4$ nanocrystals. The obtained samples for all of the measurements shown in this article are directly from synthesis without any size-selection process.

Characterization. For determining the particle sizes/shapes and crystal phase of the as-synthesized $SmVO_4$ nanocrystals, transmission electron microscopy (TEM) images and selected area electronic diffraction (SAED) patterns were performed with a JEOL JEM 1230 using an accelerating voltage of 120 kV.

Downloaded by UNIV LAVAL on October 22, 2009 | http://pubs.acs.org
Publication Date (Web): October 6, 2009 | doi: 10.1021/jp907129t

SCHEME 1: Scheme Illustrating the Formation of the $Sm(OA)_3$ and $VO_4(TOA)_3$ Complexes (i) and the Capping $SmVO_4$ Nanocrystals (ii)

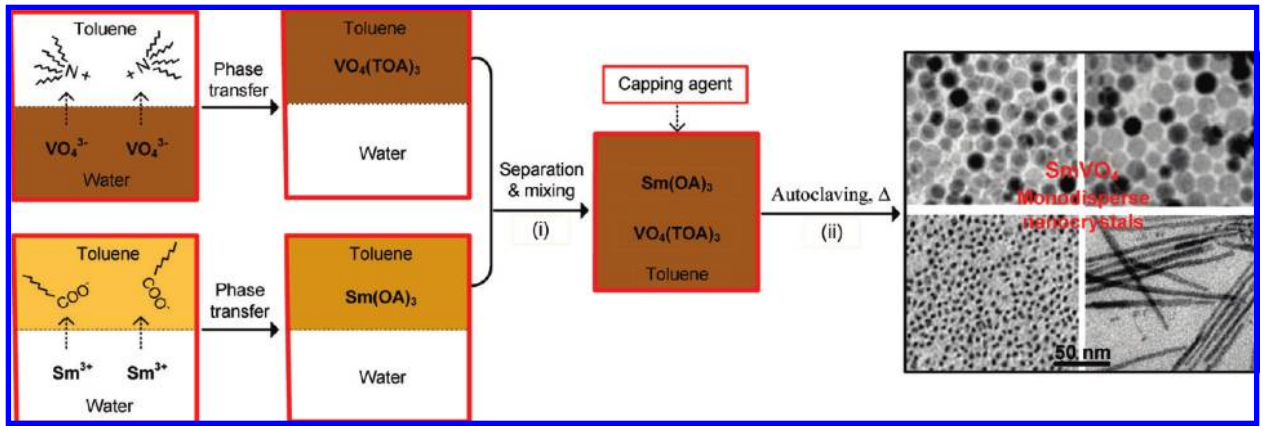

Samples were prepared by placing a drop of a dilute toluene dispersion of nanocrystals onto a 200 mesh, carbon-coated copper grid and immediately evaporating at ambient temperature. The average particle dimensions were determined by the size distribution diagrams, which were obtained from about 100−150 particles in representative TEM pictures of each sample. The crystalline phases of the products were characterized on a Bruker Smart ApexII X-ray diffractometer and operated at 1200 W power (40 kV, 30 mA) to generate Cu Kα radiation (λ = 1.5418 Å). The X-ray photoelectron spectra (XPS) were taken on a photoelectron spectrometer (Kratos Axis-Ultra) with a monochromatic X-ray source of Al Kα. The operating conditions for recording Sm 3d, V 2p, O 1s, C 1s, and N 1s high-resolution spectra was 1486.6 eV and 225 W; pass energy of 160 eV with an operating pressure of 10^{-9} Torr; and an acquisition time of 5.75 min, a pressed mixed oxide pellet under an Ar^+ bombardment. The positions of the XPS peaks were corrected using the C 1s core level taken at 285 eV as a binding energy (BE) reference. The peaks were deconvoluted by means of a standard CasaXPS software (v.2.3.13; product of CasaXPS Software Ltd., USA) to resolve the separate constituents after background subtraction. The UV−visible spectrum of the nanocrystals was recorded for the powder sample on a Hitachi U-3010 spectrometer, and pure MgO was used as a blank. The thermal analyses of the as-made $SmVO_4$ nanocrystals (∼5 mg) were carried out at a heating rate of 10 °C/min under an air flux up to 650 °C using a Perkin-Elmer TGA thermogravimetric analyzer. Fourier transform infrared absorption spectroscopy (FTIR) was measured with a FTS 45 infrared spectrophotometer using the KBr pellet technique. The specific area was calculated from the linear part of the Brunauer−Emmett−Teller equation ($P/P_o \approx 0.05-0.2$). The

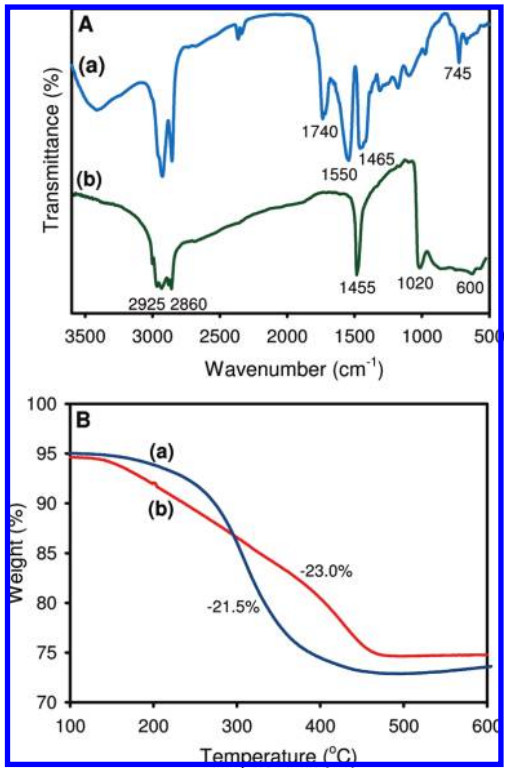

Figure 1. (A) FTIR spectra and (B) TGA curves of (a) $Sm(OA)_3$ and (b) $VO_4(TOA)_3$ complex solids.

TABLE 1: Synthesis Conditions and Corresponding Morphologies of the As-Made $SmVO_4$ Nanocrystals[a]

sample	$Sm(OA)_3$[b] [M]	$VO_4(TOA)_3$[b] [M]	OM[b] [mol]	OA[b] [mol]	shape	Size[c] [nm]	Size[d] [nm]
1	0.065	0.065	0.011		sphere	17	15.0
2	0.065	0.065		0.011	hexagon	17	15.0
3	0.065	0.065	0.002		irregular round	30	28.5
4	0.065	0.065	0.005		sphere	20	18.0
5	0.065	0.065	0.021		sphere	10	8.5
6	0.065	0.065	0.032		sphere	5	5.7
7	0.065	0.065	0.043		core	3	3.7
8	0.130	0.130	0.043		core and thin rod	3 and 3 × 10−50	
9	0.195	0.195	0.043		wire	3 × 200	
10	0.260	0.260	0.043		wire	3 × 200	

[a] All samples were synthesized by solvothermal process at 180 °C for 16 h. [b] OA^-, oleate anion; TOA^+, tetraoctylammonium cation; OM, oleylamine; OA, oleic acid. [c] Average particle size estimated by TEM. [d] Average particle size estimated by XRD.

Downloaded by UNIV LAVAL on October 22, 2009 | http://pubs.acs.org
Publication Date (Web): October 6, 2009 | doi: 10.1021/jp907129t

Downloaded by UNIV LAVAL on October 22, 2009 | http://pubs.acs.org
Publication Date (Web): October 6, 2009 | doi: 10.1021/jp907129t

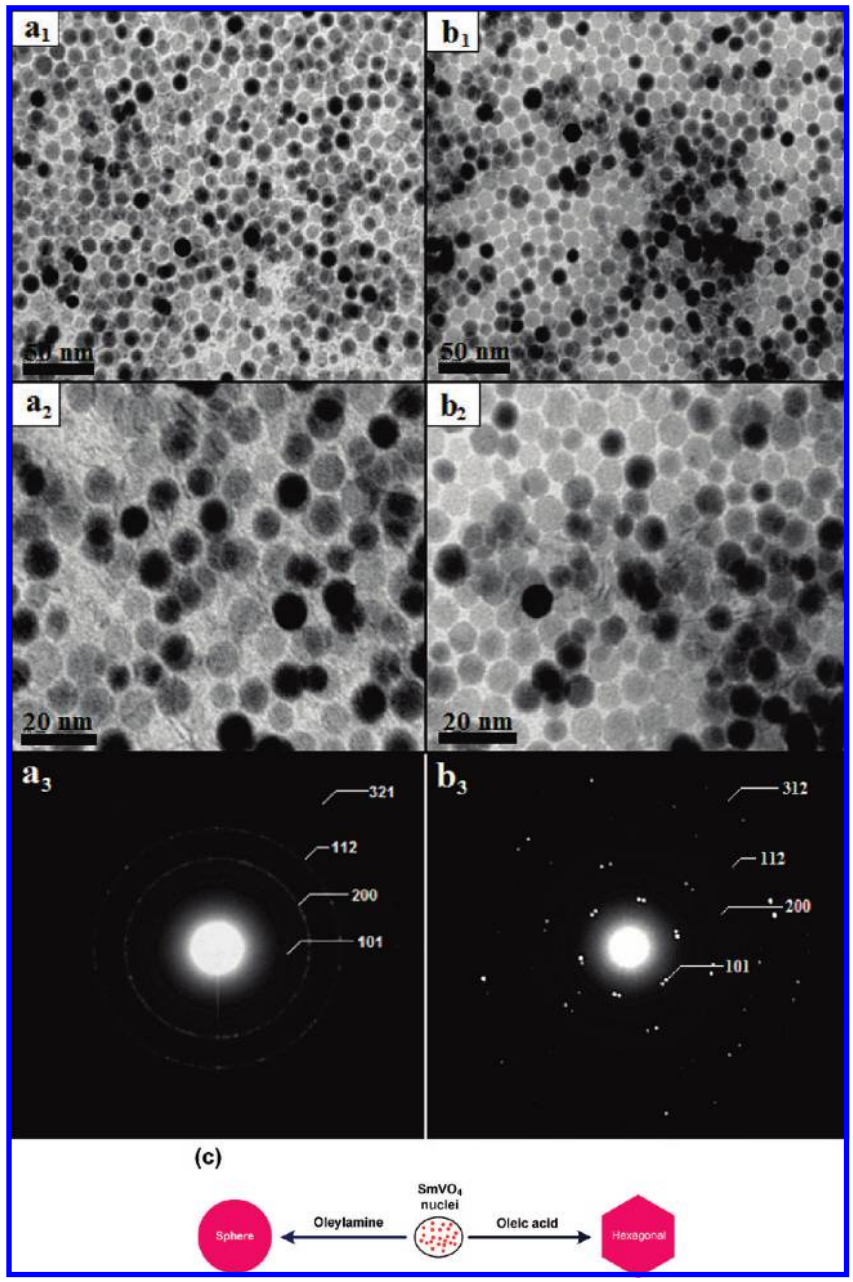

Figure 2. TEM images with different magnifications and corresponding SAED patterns of the $SmVO_4$ nanocrystals prepared using two different surfactants from the 1:1 molar mixture of $Sm(OA)_3$ and $VO_4(TOA)_3$in toluene: (a_1, a_2, a_3) using oleylamine, ~17 nm nanospheres (sample 1); (b_1, b_2, b_3) using oleic acid, ~17 nm nanohexagons (sample 2); and (c) schematic illustration for the effect of capping surfactant on the shape of the nanocrystal products.

pore diameter distribution was obtained from analysis of the desorption branch of the isotherms using the Barrett–Joyner–Halenda model.

3. Results and Discussion

In this study, $SmVO_4$ nanocrystals were synthesized using presynthesized $Sm(OA)_3$ and $VO_4(TOA)_3$ complexes as precursors, oleylamine or oleic acid as capping surfactants, and toluene as solvent. Monodisperse $SmVO_4$ nanocrystals were obtained effectively through the synthetic reaction of the two presynthesized complex precursors, $Sm(OA)_3$ and $VO_4(TOA)_3$, with a Sm/V molar ratio of 1 in toluene containing surfactant at 180 °C for 16 h. Their size and shape were also controlled by the nature and amount of capping surfactant as well as the metal complex precursor concentration. The formation of monodisperse $SmVO_4$ nanocrystals with different shapes is shown in Scheme 1 (see also the Experimental Section). The detailed synthesis conditions and various sizes and shapes of the obtained nanocrystals are summarized in Table 1. The synthetic approach for the formation of $SmVO_4$ nanocrystals consists of two steps: (i) the presynthesis of $Sm(OA)_3$ and $VO_4(TOA)_3$ complex precursors from the corresponding inorganic sources ($Sm(NO_3)_3$ and bulk V_2O_5 powders) and organic ligands (tetraoctylammonium bromide and potassium oleate), which are depicted by eqs 1 and 2, and (ii) the formation of $SmVO_4$ nanocrystals from the presynthesized $Sm(OA)_3$ and $VO_4(TOA)_3$ complexes in toluene containing capping molecules under solvothermal treatment, as described in eq 3 (see Experimental Section).

$$Sm^{3+}(aqueous) + 3OA^{-}(toluene) \rightarrow Sm(OA)_3(toluene) \quad (1)$$

$$VO_4^{3-}(aqueous) + 3TOA^{+}(toluene) \rightarrow VO_4(TOA)_3(toluene) \quad (2)$$

The formation of the complex precursor solids, $Sm(OA)_3$ and $VO_4(TOA)_3$ (after toluene elimination), was supported by the FTIR and TGA results (Figure 1). The FTIR spectra of the $Sm(OA)_3$ and $VO_4(TOA)_3$ complexes show the absorption bands at 745 and 500−700 cm^{-1}, which are assigned to the stretching vibrations of the Sm−O and V−O bonds, respectively.[51,52] The well-defined IR bands at 2925−2860 cm^{-1} are characteristic of the symmetric, asymmetric methyl and methylene stretches of the alkyl chains. The absorption bands at 1465−1550 cm^{-1} are attributed to the stretching vibrations of the carboxylate groups of oleate ligands (Figure 1A-a).[52] As shown in Figure 1A-b, an IR band at 1455 cm^{-1} is attributed to the stretching vibrations of the ammonium cation groups ($\equiv N^+$) of TOA^+.[51] Furthermore, the TGA data for these $Sm(OA)_3$ and $VO_4(TOA)_3$ complex solids exhibit mass losses of 21.5 and 23.0%, respectively, in the temperature range 150−470 °C, which are attributed to the decomposition and combustion of organic OA^- and TOA^+ ligands, respectively. This indicates the formation of the $Sm(OA)_3$ and $VO_4(TOA)_3$ complexes.

To study the effect of the nature of surfactant on the size and shape of nanocrystals, two surfactants with different functional groups, such as amines or acids, having different binding strengths were used. In general, oleylamine possesses a stronger binding strength (e.g., as nonselective surfactant) to the particle surface compared to that of oleic acid (e.g., as selective surfactant). In this work, we used either oleylamine (OM) or oleic acid (OA); the other reaction conditions remained unchanged. $SmVO_4$ nanocrystals were typically synthesized by mixing the equimolar quantity of the two presynthesized complexes ($[Sm(OA)_3] = [VO_4(TOA)_3] = 0.065$ M) in toluene containing capping surfactant (0.129 M) at 180 °C for 16 h. The reaction mixture consisted of the corresponding 4:1 molar ratio of surfactant and (Sm + V) complex precursors.

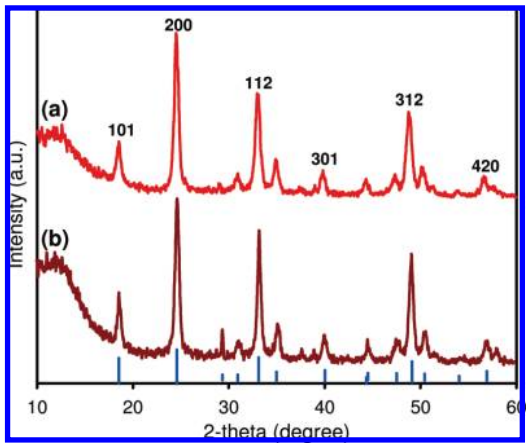

Figure 3. XRD patterns of the as-synthesized $SmVO_4$ samples: (a) nanospheres and (b) nanohexagons. Vertical bars denote the peak positions and relative intensities of the tetragonal zircon-type structure (JCPDS no. 17-0876).

Figure 2 displays TEM images of the $SmVO_4$ nanocrystals at two different magnifications obtained using two different surfactants (e.g., oleylamine and oleic acid) and the corresponding SAED patterns. When oleylamine was used, (see Figure $2a_1$ and a_2), nanospheres ∼17 nm in diameter were obtained. However, using oleic acid as the capping surfactant instead of oleylamine under the same synthesis conditions, hexagonal-like $SmVO_4$ nanocrystals with no significant change in particle size (∼17 nm in diameter) were formed (Figure $2b_1$ and b_2). Both nanospheres and nanohexagons exhibited a high uniformity and were assembled to form the ordered nanostructures. The SAED patterns taken from individual spherical and hexagonal nanocrystals are shown in Figure $2a_3$ and b_3. The SAED results revealed that both samples are indexed to a tetragonal $SmVO_4$ single crystal with strong spots originating from the (101), (200), (112), and (312) planes, which are consistent with the X-ray diffraction (XRD) results (see below). It is clear that capping surfactants have distinct effects on the shape of the final product during the crystal-growth process, depending on their nature, as also depicted in Figure 2c. Furthermore, when extending the reaction time (180 °C for 24 h instead of 16 h), the morphology of both the spherical and hexagonal nanocrystal products did not change significantly; however, a broadening of the size distribution was observed (Supporting Information S-Figure 1). The particle size distributions further broadened, suggesting the desired balance between nucleation and growth under these reaction conditions.[53]

Figure 3 show the XRD patterns of the as-synthesized $SmVO_4$ nanospheres and nanohexagons. Both samples display the XRD peaks, which are well-indexed to a tetragonal zircon-type structure with lattice contents of $SmVO_4$: $a = b = 7.265$ Å, $c = 6.389$ Å ($Fm3\,hm$, JCPDS no. 17-0876).[54] No XRD peaks correspond to single metal oxides of V_2O_5,[51] and Sm_2O_3[52] was detected, indicating that the pure tetragonal zircon-type structure of $SmVO_4$ nanocrystals can be achieved by this method. The well-resolved diffraction and intense broadening of the peaks indicate a high crystallinity and a small particle size of the nanocrystal products. The average particle size of these $SmVO_4$ nanocrystals calculated from the (200) peak[55] using the Scherrer formular are ∼13.5 nm, which is consistent with the TEM results. It can also be concluded that the formation of the pure tetragonal $SmVO_4$ phase results in complete reaction of the 1:1 ratio of Sm^{3+} cation and VO_4^{3-} anion monomers in the bulk solution during the synthesis.

To investigate the role of oleylamine (OM) in the formation of $SmVO_4$ nanoparticles, one synthesis without OM in the bulk solution was carried out. Without OM, only irregular nanocrystals with aggregated pearl-chain-like structures were formed. Furthermore, these nanocrystals were not dispersed in nonpolar solvents, also indicating their polyparticle sizes (Supporting Information S-Figure 2). However, when an appropriate amount of surfactant (0.025−0.43 M) was added to the synthesis solution, monodisperse nanocrystals with controlled size could be obtained, depending on the OM concentration. To gain further insight into the mechanistic aspect of this process, a series of experiments was performed with different oleylamine (OM) concentrations in the synthesis solution: 0.025, 0.060, 0.129, 0.230, 0.034, and 0.43 M, corresponding to the OM/(Sm + V) molar ratios (denoted as OM/P) of 0.8, 2, 4, 8, 12, and 17, whereas the other components and reaction conditions remained

Downloaded by UNIV LAVAL on October 22, 2009 | http://pubs.acs.org
Publication Date (Web): October 6, 2009 | doi: 10.1021/jp907129t

Downloaded by UNIV LAVAL on October 22, 2009 | http://pubs.acs.org
Publication Date (Web): October 6, 2009 | doi: 10.1021/jp907129t

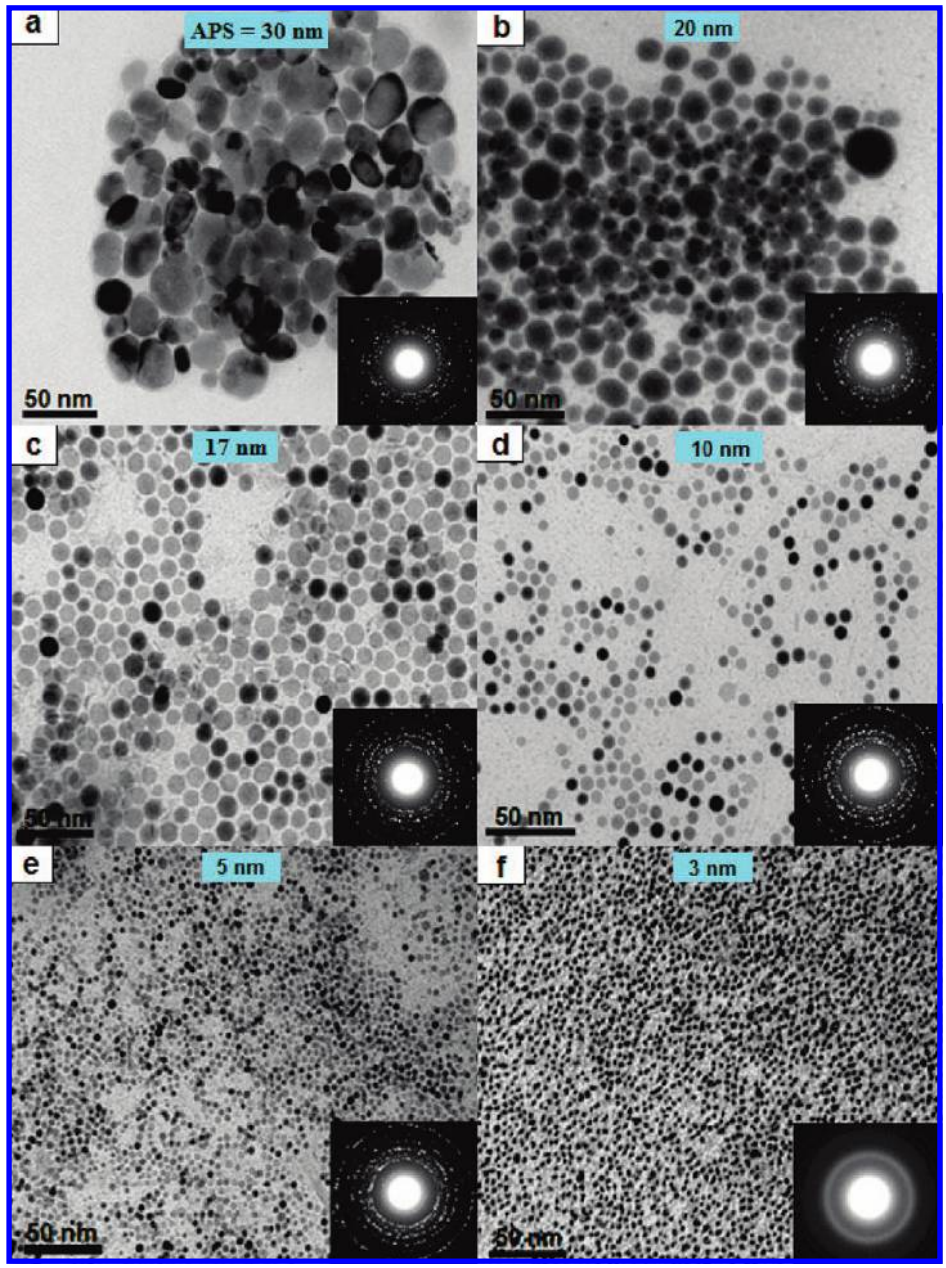

Figure 4. Effect of the oleylamine concentration in the bulk solution on the particle size (average particle size denoted as APS). TEM images and corresponding inset SAED patterns of the $SmVO_4$ nanocrystals synthesized using different molar ratios of oleylamine/precursor (OM/P): (a) OM/P = 0.8, ~30 nm roundlike nanocrystals (sample 3); (b) OM/P = 2, ~20 nm nanospheres (sample 4); (c) OM/P = 4, ~17 nm nanospheres (sample 1); (d) OM/P = 8, ~10 nm nanospheres (sample 5); (e) OM/P = 12, ~5 nm nanospheres (sample 6); and (f) OM/P = 17, ~3 nm nanocores (sample 7).

unchanged (e.g., $[Sm(OA)_3] = [VO_4(TOA)_3] = 0.065$ M, 80 mL toluene, and at 180 °C for 16 h). It was found that the $SmVO_4$ nanocrystal size varies as a function of the OM concentration. Figure 4 shows representative TEM images of these samples varying from ~30 to ~3 nm. At low OM concentrations in the synthesis solution (for example, OM/P = 0.8), irregular particles with an average diameter of 30 nm were observed (Figure 4a). When the OM/P ratio was increased to 2, uniform 20 nm-sized nanospheres in company with some irregularly large spheres were found (Figure 4b). When the OM/P ratio reached 4, the exclusive formation of uniform nanospheres with an average diameter of 17 nm was produced (Figure 4c). Furthermore, as the OM/P ratio increased from 4 to 8, 12, and then 17, the spherical particle size gradually decreased from 17 to 10, 5, and then 3 nm, respectively (Figure 4d−f).

These results clearly indicate that irregular and large particle sizes of nanocrystals were formed at low OM surfactant concentrations (≤0.25 M or OM/P = 0.8). At higher OM surfactant concentrations in the synthesis reaction, from 0.025 to 0.43 M (e.g., OM/P ratio from 0.8 to 17), the spherical crystal size is decreased from 30 to 3 nm.

The reason for this behavior may be the high degree of surfactant protection and stabilization of nanocrystals with increasing OM concentrations in the bulk reaction solution. The larger and irregular sizes of the nanocrystals at low OM concentrations as compared to those obtained at high OM concentrations may result in insufficient coverage of the nanocrystal surface and induce their aggregation. Furthermore, in all the cases, spherical nanocrystals were produced. The formation of spherical NPs could be due to the nonselective surfactant character of oleylamine (OM).[18,56]

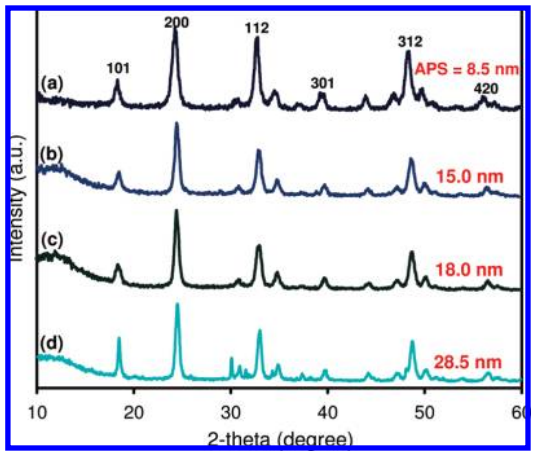

Figure 5. XRD patterns of the $SmVO_4$ nanocrystals synthesized using different molar ratios of oleylamine and precursor (OM/P). OM/P = (a) 8, (b) 4, (c) 2, and (d) 0.8. The average particle sizes (APS) were calculated from the (200) peak using the Debye−Sherrer equation.

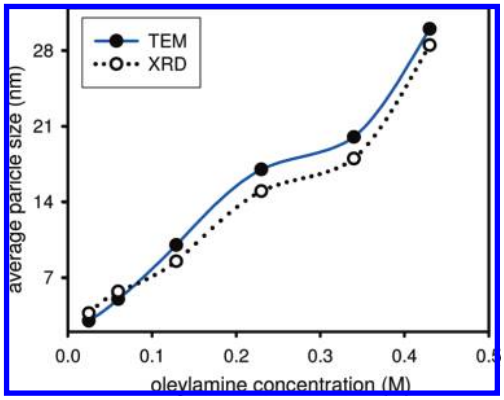

Figure 6. Effect of oleylamine concentration on the average particle size of $SmVO_4$ nanocrystals estimated by TEM (solid curve) and XRD (dotted curve).

The corresponding SAED patterns (inset of Figure 4) of individual $SmVO_4$ particles exhibit the well-defined, single-crystalline structure. The XRD patterns of the $SmVO_4$ nanocrystals synthesized using different oleylamine concentrations are also shown in Figure 5. Their average particle sizes were further calculated from the (200) XRD peak using the Debye−Sherrer equation. The particle size is decreased from 28.5, 18, and 15.0 to 8.5 nm when increasing the OM/P molar ratio from 0.8, 2, and 4 to 8. The nanocrystal sizes estimated using TEM and XRD techniques is presented in Figure 6. A similar trend and no significant difference in particle size using these two techniques were observed, indicating that each individual particle is a single crystal.[57]

The influence of metal complex precursor concentrations on size and shape of final nanocrystal products was also systematically studied. A series of $SmVO_4$ nanocrystals was synthesized at the same reaction conditions: Sm/V of 1, oleyamine/(Sm + V) complex precursors of 4 (denoted as OM/P), and at 180 °C for 16 h; however, using different initial precursor concentrations of $Sm(OA)_3$ and $VO_4(TOA)_3$ from low to high (Sm + V) concentrations; for example, from 0.065 to 0.130, 0.195, and 0.260 M.

Representative TEM images and corresponding SAED patterns of the resulting nanocrystals are shown in Figure 7. It is clear that the shape evolution of nanocrystal products is as a function of initial complex precursor concentration, from nanocores to nanowires. This observation also indicates that low monomer concentrations favor isotropic growth, whereas high monomer concentrations favor anisotropic growth.[58,59] At low precursor monomer concentrations (e.g., 0.065 M), almost core-shaped nanocrystals with an average diameter of 3 nm were produced (Figure 7a). It is also noted that at the lower monomer concentration (<0.065 M), no formation of nanocrystals was observed (Supporting Information S-Figure 3). This could be due to the monomer concentration being lower than that required for the formation of nuclei. Furthermore, under the same synthesis conditions, increasing the precursor monomer concentration to 0.130 M, about 40% primary thin nanorods 3 nm in width and ∼10−50 nm in length was observed, although nanocores were still the exclusive products (Figure 7b).

When the precursor monomer concentration was increased from 0.130 to 0.195 M, essentially no nanocores were observed. Concomitantly, only the individual nanowires grew along their longitudinal axis, yielding nanowires ∼3 nm in width and 200 nm in length, and having an aspect ratio (length/width) of ∼ 66 (Figure 7c). This indicates a complete conversion from nanocores into nanowires at this monomer concentration. Finally, when the precursor monomer concentration was increased further to 0.260 M, a large number of nanowires were produced, but no obvious change in their morphology (constant aspect ratio) was observed, suggesting that the equilibrium of growth kinetics may be established at this range of monomer concentrations (Figure 7d). These results reveal that the shape evolution from 3 nm-sized nanocores to 3 nm × 200 nm-sized nanowires can be controlled by increasing the precursor monomer concentration from 0.065 to 0.260 M, which is strongly associated with the increase in chemical potential in the bulk solution as well as the dominant oriented attachment for the formation of nanowires, as also reported recently by our group.[52,60]

The corresponding SAED patterns (inset of Figure 7) of these nanocrystal samples also exhibit their single-crystalline structure. The XRD patterns of the as-synthesized nanocores and nanowires also show a pure tetragonal phase $SmVO_4$ structure (Figure 8). No diffraction peaks from any corresponding single metal oxide species are detected. The intense broadening of the peaks is caused by the small particle sizes. The particle size of nanocores calculated from the (200) peak[55] using the Scherrer formula is about 3.7 nm, which is nearly equal to that observed by the TEM result (Figures 7a). It is important to note that the relative intensity of the (200) diffraction peak of the nanowires is much higher than that of the nanocores, suggesting their elongation along the [200] direction.

Schematic illustration for the formation mechanism of $SmVO_4$ nanocrystals and their size and shape evolution under different reaction stages in the whole synthetic process can be overall summarized in detail in Scheme 2.

Elemental dispersive spectrum (EDS) analysis of these as-made $SmVO_4$ nanospheres (Figure 9A) qualitatively indicates that the sample is elementally composed solely of Sm, V, and O. Further evidence for the chemical composition and oxidation states on the surface of the as-made and calcined samarium orthovanadate nanospheres was analyzed by the XPS technique. The survey XPS spectra of these samples in a wide energy range are shown in Figure 9B. Core levels of Sm 3d, V 2p, O 1s, N 1s, and C 1s can be identified. However, the intense N 1s and C 1s peaks of the as-made as compared to those of the calcined samples can be assigned to the oleylamine ligand capped on the nanocrystal surface. The molar ratio of Sm/V determined from the surface chemical composition of both the as-made and calcined samples was very close to 1:1, agreeing with the

Downloaded by UNIV LAVAL on October 22, 2009 | http://pubs.acs.org
Publication Date (Web): October 6, 2009 | doi: 10.1021/jp907129t

Downloaded by UNIV LAVAL on October 22, 2009 | http://pubs.acs.org
Publication Date (Web): October 6, 2009 | doi: 10.1021/jp907129t

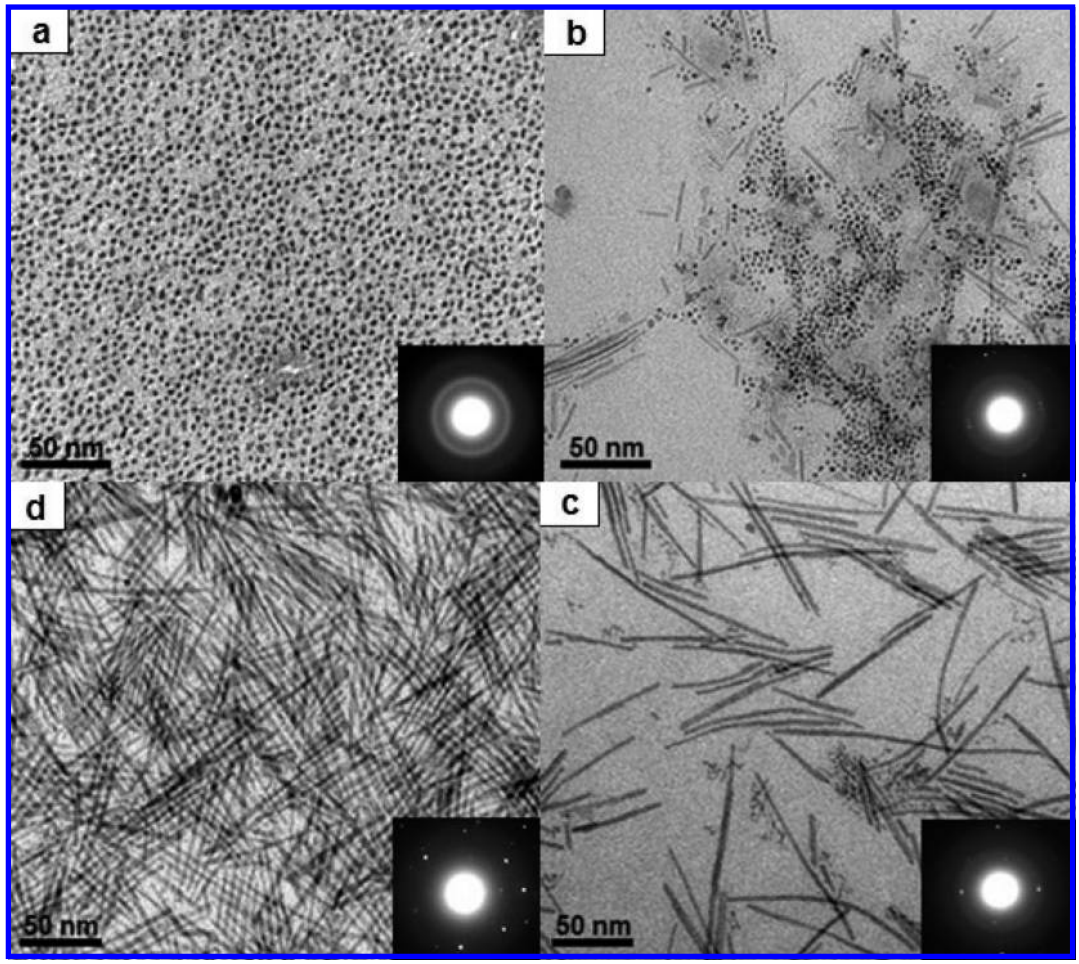

Figure 7. Effect of the monomer precursor concentration in the synthesis solution on the shape of the nanocrystals, from nanocores to nanowires. TEM images and corresponding inset SAED patterns of the $SmVO_4$ nanocrystals synthesized using different precursor concentrations, while keeping the Sm/V molar ratio at 1. ($C = [Sm(OA)_3] = [VO_4(TOA)_3]$): (a) $C = 0.065$ M, 3 nm nanocores (sample 7); (b) $C = 0.130$ M, mixture of 3 nm nanocores and 3 nm × 10−50 nm thin nanorods (sample 8); (c) $C = 0.195$ M, 3 nm × 200 nm nanowires (sample 9); and (d) $C = 0.260$ M, 3 nm × 200 nm nanowires (sample 10).

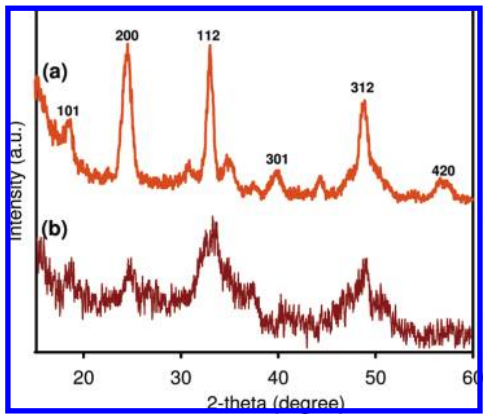

Figure 8. XRD patterns of the as-synthesized $SmVO_4$ samples: (a) nanowires (sample 10) and (b) nanocores (sample 7).

SCHEME 2: The Overall Schematic Illustration of the Size and Shape Control of Alkyl-Capped $SmVO_4$ Nanocrystals

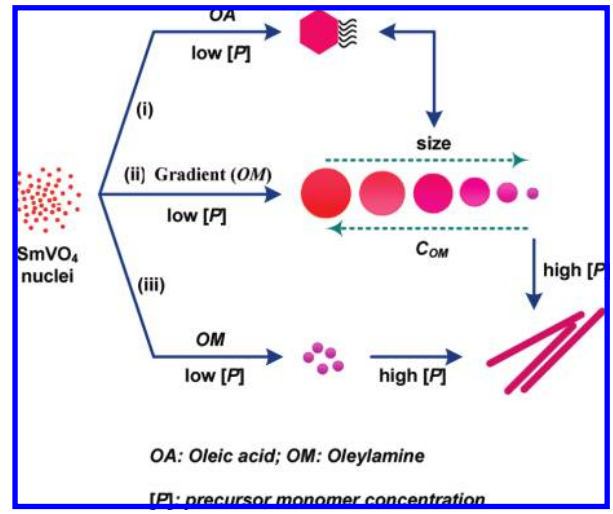

formula of $SmVO_4$. It is interesting to note that no difference of the Sm 3d and V 2p XPS spectra before and after calcination at 550 °C of these samples was observed, suggesting no significant change in the samarium and vanadium oxidation state upon this thermal treatment. As shown in Figure 10A and B, the Sm 3d and V 2p XPS spectra of both the as-made and calcined nanospherical $SmVO_4$ samples exhibit only one oxidation state of Sm^{3+} and V^{5+} at the nanoscale and even in a ultrahigh vacuum for XPS measurements. The Sm^{3+} $3d_{5/2,3/2}$ peaks at 10834.0−1111.0 eV and the V^{5+} $2p_{3/2,1/2}$ peaks at 517.5−535.5 eV were observed.[51,52] Both spectra show that non-XPS peaks corresponding to Sm^{2+} and V^{4+} were detected, indicating the formation of a stable tetragonal $SmVO_4$ structure.

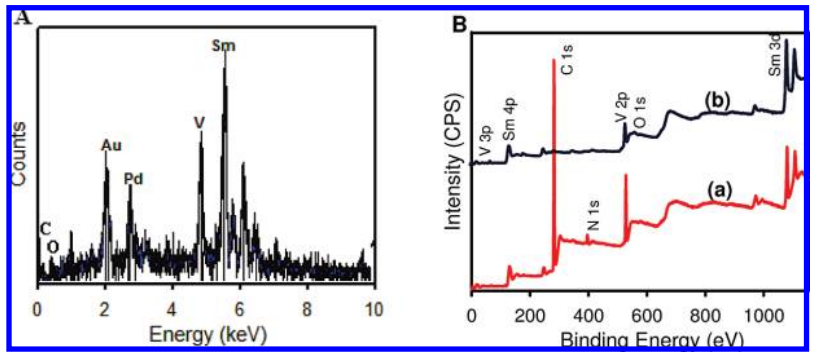

Figure 9. (A) EDS spectrum of the as-synthesized $SmVO_4$ nanospheres and (B) survey XPS spectra of the $SmVO_4$ nanospheres before (a) and after (b) calcination at 550 °C.

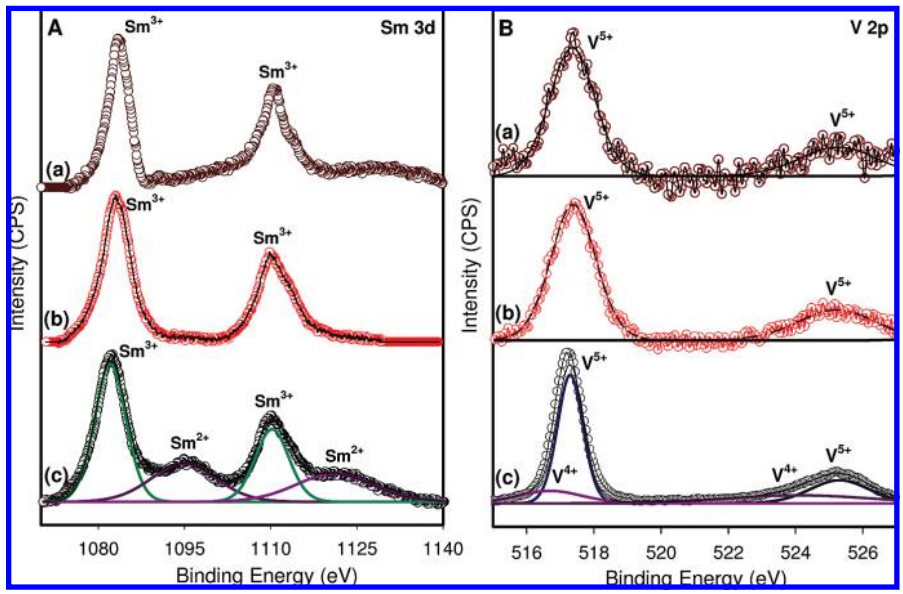

Figure 10. (A) Sm 3d XPS spectra of (a) the as-made $SmVO_4$ nanospheres, (b) the calcined $SmVO_4$ nanospheres, and (c) the calcined Sm_2O_3 nanospheres. (B) V 2p XPS spectra of (a) the as-made $SmVO_4$ nanospheres, (b) the calcined $SmVO_4$ nanospheres, and (c) the calcined V_2O_5 nanospheres.

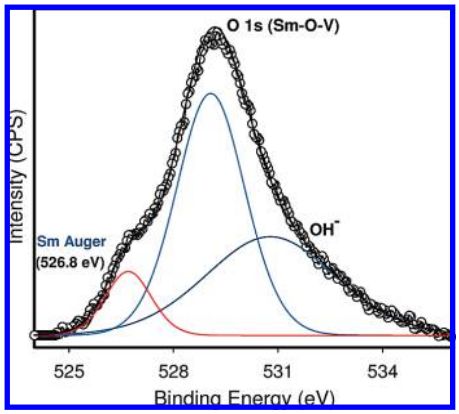

Figure 11. O 1s XPS spectrum of the as-made $SmVO_4$ nanospheres.

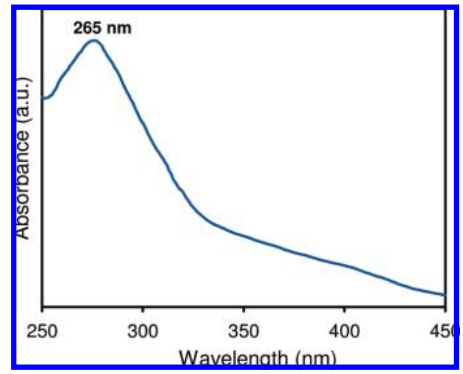

Figure 12. UV−visible absorption spectrum of the as-made $SmVO_4$ nanospheres.

However, for the single spherical nanovanadia[51] and nanosamaria[52] samples that were synthesized following the methods reported previously by our group,[51,52] the Sm 3d and V 2p XPS spectra exhibit two additional weak peaks at 1095.9−1121.3 eV for Sm^{2+} $3d_{5/2,3/2}$ and at 516.2−524.1 eV for V^{4+} $2p_{5/2,3/2}$, as compared to those of the mixed oxide $SmVO_4$ nanospherical sample. This difference is due to the fact that, for each single metal oxide, the single Sm−O−Sm bonds in Sm_2O_3, and the V−O−V bonds in V_2O_5 allow the multiple oxidation states, whereas for the mixed metal oxides, the presence of mixed Sm−O−V bonds in $SmVO_4$ requires only the formation of Sm^{3+}−V^{5+} species.[36,38,61,62]

Figure 11 shows the O 1s XPS spectrum of the as-made $SmVO_4$ nanospheres. A peak at 530.5 eV is attributed to both O−Sm and O−V bonds in the tetragonal $SmVO_4$ lattice,[63] which consists of VO_4 tetrahedra that share corners and edges with SmO_8 dodecahedra.[64,65] The smaller peak at 532.2−533.1 eV is ascribed to the presence of hydroxyl species or adsorbed water

Downloaded by UNIV LAVAL on October 22, 2009 | http://pubs.acs.org
Publication Date (Web): October 6, 2009 | doi: 10.1021/jp907129t

Downloaded by UNIV LAVAL on October 22, 2009 | http://pubs.acs.org
Publication Date (Web): October 6, 2009 | doi: 10.1021/jp907129t

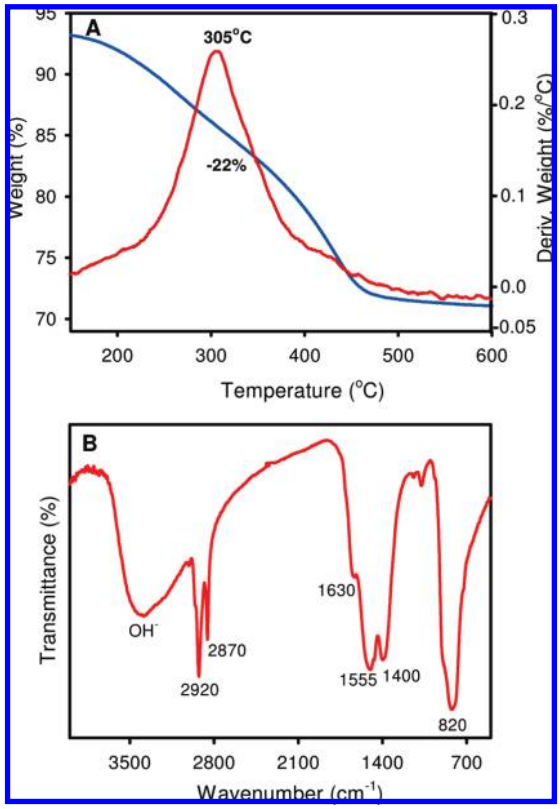

Figure 13. (A) TGA−DTA curves and (B) FTIR spectrum of the oleylamine-capped $SmVO_4$ nanospheres (sample 1 in Table 1).

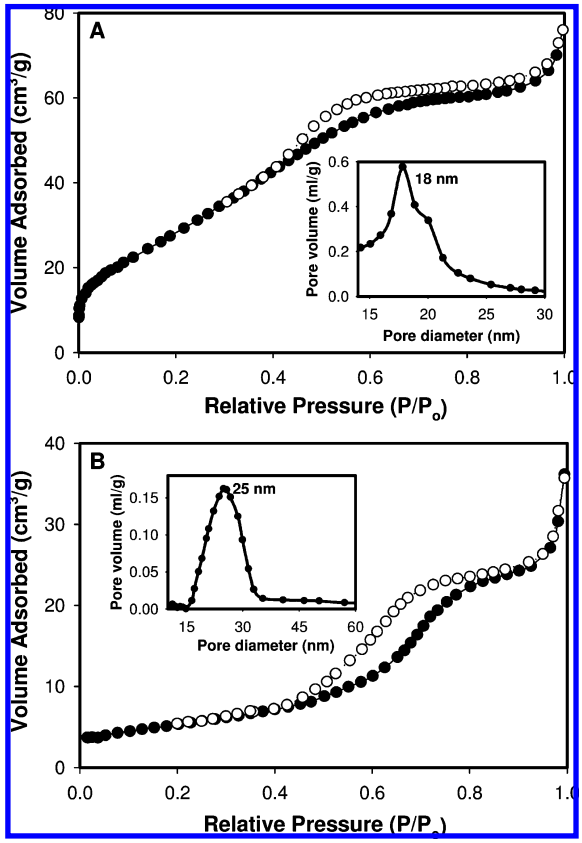

Figure 14. Nitrogen adsorption (filled symbols) and desorption (open symbols) isotherms and inset BJH pore diameter distribution of (A) the calcined $SmVO_4$ nanospheres (sample 1 in Table 1) and (B) the calcined $SmVO_4$ nanowires (sample 10 in Table 1).

on the nanocrystal surface. In addition, the appearance of one broader peak at ∼526.8 eV could be assigned to a Sm Auger peak.[66]

The UV−visible absorption spectrum of the as-synthesized $SmVO_4$ nanosphere sample was recorded to characterize its optical properties (Figure 12). It can be seen that a strong absorption peak at 265 nm is present, which is attributed to the charge transfer from the oxygen ligands to the central vanadium atom inside the VO_4^{3-} groups in the samarium orthovanadate.[67] The TGA−DTA curves (Figure 13A) of the oleylamine-capped $SmVO_4$ nanospheres (sample 1 in Table 1) exhibit a weight loss of 22%, appearing around 150−550 °C, accompanied by an exothermic peak at 305 °C, which are related to the decomposition and combustion of oleylamine molecules bounded on the particle surfaces during heating.

The FTIR spectrum (Figure 13B) of this as-made sample shows bands at 2920−2870 and 1630 cm^{-1} that are assigned to the C−H and C═C stretching modes, respectively,[51] of alkyl chains in oleylamine. The band at 1440 cm^{-1} is attributed to the N−H bending and N−C stretching modes of $-NH_2$ groups in oleylamine capped on the $SmVO_4$ nanocrystal surface.[51] The IR bands at 820 cm^{-1} are attributed to the Sm−O−V vibrations of $SmVO_4$.[61] Residual water and a hydroxide group are detected with a large band around 3500 cm^{-1}, corresponding to the O−H stretching frequency due to the bending vibration of associated water. These data suggest oleylamine molecules bound to the nanocrystal surface and further confirm that the $SmVO_4$ is formed under this synthetic condition.

Figure 14 shows the N_2 adsorption/desorption isotherms and pore diameter distributions of the calcined $SmVO_4$ nanosphere and nanowire samples. It can be seen from Figure 14A and B that both samples exhibit a type IV isotherm. Futhermore, the H_3 hysteresis loop at the 0.4−1.0 P/P_o and the H_1 hysteresis loop at the 0.4−0.8 P/P_o pressure range for the nanosphere and nanowire samples, respectively, indicate the presence of the mesopore structure in these samples.[68,69] The pore diameters (inset of Figures 13A and B) calculated using the BJH method are about 19.5 and 57.0 nm, respectively, which originated from the interparticle space formed by the aggregation of the $SmVO_4$ nanocrystals upon calcination. The BET specific surface area of the nanospheres is 110 $m^2\ g^{-1}$, which is higher than that of the nanowires (70 $m^2\ g^{-1}$). This could be logically due to the difference in the sphere and wire shapes of these samples.

It is well-known that the shape and size of the well-defined nanocrystals are key factors that determine their chemical and physical properties. For example, single CeO_2 nanospheres with an even higher surface area and smaller particle size have a lower catalytic activity for the CO oxidation reaction as compared to that of single CeO_2 nanorods; these unusual results inspire us to hope that specific planes are, indeed, a determining factor that will prove useful.[70]

This new approach for the shape-controlled synthesis of this type of mixed metal oxide $SmVO_4$ nanocrystals in the present work is an important role for designing novel catalysts with desired performance. Further work to gain insight into the study of the catalytic properties of these $SmVO_4$ nanomaterials with various shapes as well as novel metal-doped $SmVO_4$ nanocrystals are in progress in our laboratory.

4. Conclusion

We have developed a new approach for the controllable synthesis of monodisperse and well-crystallized $SmVO_4$ nanocrystals with various shapes from the reaction of $Sm(OA)_3$ and $VO_4(TOA)_3$ complexes in toluene in the presence of a capping

surfactant (either oleylamine or oleic acid) through a solvothermal pathway. The $Sm(OA)_3$ and $VO_4(TOA)_3$ complex precursors were presynthesized from inexpensive inorganic sources and organic ligands. This solvothermal approach is simple and reproducible and employs a relatively mild reaction temperature. By varying the reaction parameters, such as the nature and amount of surfactant and the metal complex precursor concentration, the different morphologies of the $SmVO_4$ nanocrystals can be easily controlled. The formation of the $SmVO_4$ nanocrystals with spherical and hexagonal shapes uses oleylamine and oleic acid as the capping surfactant, respectively. It could be due to the different binding strengths of these surfactants (as nonselective and selective surfactant). Tuning the surfactant concentration in the synthesis solution is a crucial step for the discrete, monodisperse, and size-controlled $SmVO_4$ nanospheres. Increasing the oleylamine concentration from 0.025 to 0.43 M induces a decrease in the particle size from ~30 to ~3 nm. Furthermore, the shape evolution of nanocrystals was also controlled by tuning the initial metal complex precursor concentration. This is associated with an increase in the chemical potential in bulk solution. At the low metal complex precursor concentration range from 0.065 to 0.130 M, only nanocores or a mixture of nanocores and primary thin nanorods of the $SmVO_4$ crystals were produced. At the higher precursor concentrations range from 0.195 to 0.260 M, uniform $SmVO_4$ nanowires ~3 nm in diameter and ~200 nm in length were obtained.

The SAED patterns of the $SmVO_4$ nanocrystal samples showed a set of sharp spots characteristic of single crystalline structure, and the strong diffraction rings indexed accordingly with the pure tetragonal structure determined by the XRD patterns. The XPS results reveal only one oxidation state for Sm^{3+} and V^{5+} on the $SmVO_4$ nanocrystal surface, whereas two oxidation states of Sm^{3+}/Sm^{2+} and V^{5+}/V^{4+} were found for the single samarium oxide and vanadium oxide nanospheres, respectively. We believe that this approach can also be extended for the synthesis of other uniform rare earth orthovanadate, molybdate, and tungstate nanocrystals in tailoring different sizes and shapes.

Acknowledgment. This work was supported by the Natural Sciences and Engineering Research Council of Canada (NSERC) through a strategic grant.

Supporting Information Available: Additional information as noted in text. This material is available free of charge via the Internet at http://pubs.acs.org.

References and Notes

(1) Redl, F. X.; Cho, K. S.; Murray, C. B.; O'Brien, S. *Nature* **2003**, *423*, 968–971.
(2) Zarur, A. J.; Ying, J. Y. *Nature* **2000**, *403*, 65–67.
(3) Schrinner, M.; Ballauff, M.; Talmon, Y.; Kauffmann, Y.; Thun, J.; Möller, M.; Breu, J. *Science* **2009**, *323*, 617–620.
(4) Ferrando, R.; Jellinek, J.; Johnston, R. L. *Chem. Rev.* **2008**, *108*, 845–910.
(5) Maye, M. M.; Nykypanchuk, D.; Cuisinier, M.; Lelie, D.; Gang, O. *Nat. Mater.* **2009**, *8*, 388–391.
(6) Cushing, B. L.; Kolesnichenko, V. L.; O'Connor, C. J. *Chem. Rev.* **2004**, *104*, 3893–3946.
(7) Dahl, J. A.; Maddux, B. L. S.; Hutchison, J. E. *Chem. Rev.* **2007**, *107*, 2228–2269.
(8) Kwon, S. G.; Hyeon, T. *Acc. Chem. Res.* **2008**, *41*, 1696–1709.
(9) Wang, X.; Peng, Q.; Li, Y. *Acc. Chem. Res.* **2007**, *40*, 635–643.
(10) Mutin, P. H.; Vioux, A. *Chem. Mater.* **2009**, *21*, 582–596.
(11) Sun, Y.; Xia, Y. *Science* **2002**, *298*, 2176–2179.
(12) Tian, N.; Zhou, Z. Y.; Sun, S. G.; Ding, Y.; Wang, Z. L. *Science* **2007**, *316*, 732–735.
(13) Jun, Y. W.; Seo, J. W.; Cheon, J. *Acc. Chem. Res.* **2008**, *41*, 1630–1640.
(14) Polshettiwar, V.; Baruwati, B.; Varma, R. S. *ACS Nano* **2009**, *3*, 728–736.
(15) El-Sayed, M. A. *Acc. Chem. Res.* **2004**, *37*, 326–333.
(16) Yang, S. M.; Kim, S. H.; Lima, J. M.; Yi, G. R. *J. Mater. Chem.* **2008**, *18*, 2177–2190.
(17) Liang, X.; Gao, L.; Yang, S.; Sun, J. *Adv. Mater.* **2009**, *21*, 1–4.
(18) Watt, J.; Young, N.; Haigh, S.; Kirkland, A.; Tilley, R. D. *Adv. Mater.* **2009**, *21*, 1–6.
(19) Si, R.; Zhang, Y. W.; You, L. P.; Yan, C. H. *Angew. Chem.* **2005**, *117*, 3320–3324.
(20) Park, J.; Koo, B.; Yoon, K. Y.; Hwang, Y.; Kang, M.; Park, J. G.; Hyeon, T. *J. Am. Chem. Soc.* **2005**, *127*, 8433–8440.
(21) Niu, W.; Zheng, S.; Wang, D.; Liu, X.; Li, H.; Han, S.; Chen, J.; Tang, Z.; Xu, G. *J. Am. Chem. Soc.* **2009**, *131*, 697–703.
(22) Peng, Z. A.; Peng, X. *J. Am. Chem. Soc.* **2001**, *123*, 1389–1395.
(23) Au, C. T.; Zhang, W. D. *J. Chem. Soc. Faraday Trans.* **1997**, *93*, 1195–1204.
(24) Tsipis, E. V.; Patrakeev, M. V.; Kharton, V. V.; Vyshatko, N. P.; Frade, J. R. *J. Mater. Chem.* **2002**, *12*, 3738–3745.
(25) Chen, F.; Wang, X.; Li, S.; Fu, G.; Wang, K.; Lu, Q.; Shen, D.; Nie, R.; Ma, H. *J. Appl. Phys.* **2003**, *94*, 4708–4710.
(26) Picardi, G.; Varsano, F.; Decker, F.; Krasovec, U. O.; Surca, A.; Orel, B. *Electrochim. Acta* **1999**, *44*, 3157–3164.
(27) Yu, M.; Lin, J.; Wang, S. B. *Appl. Phys. A: Mater. Sci. Process.* **2005**, *80*, 353.
(28) Fields, R. A.; Birnbaum, M.; Fincher, C. L. *Appl. Phys. Lett.* **1987**, *51*, 1885–1856.
(29) Liu, J. F.; Yao, Q. H.; Li, Y. D. *Appl. Phys. Lett.* **2006**, *88*, 173119.
(30) Gaur, K.; Lal, H. B. *J. Mater. Sci. Lett.* **1983**, *2*, 744.
(31) Stouwdam, J. W.; Raudsepp, M.; Veggel, F. V. *Langmuir* **2005**, *21*, 7003–7008.
(32) Matta, J.; Courcot, D.; Abi-Aad, E.; Aboukais, A. *Chem. Mater.* **2002**, *14*, 4118–4125.
(33) Au, C. T.; Zhang, W. D.; Wan, H. L. *Catal. Lett.* **1996**, *37*, 241–246.
(34) Sugunan, S.; Renuka, N. K. *Bull. Chem. Soc. Jpn.* **2002**, *75*, 463–471.
(35) Mamedov, E. A.; Corberfin, V. C. *Appl. Catal., A* **1995**, *127*, 1–40.
(36) Barbero, B. P.; Cadus, L. E. *Appl. Catal., A* **2003**, *244*, 235–249.
(37) Li, K. T.; Chi, Z. H. *Appl. Catal., A* **2001**, *206*, 197–203.
(38) Barbero, B. P.; Cadus, L. E. *Appl. Catal., A* **2002**, *234*, 245–258.
(39) Lee, I.; Morales, R.; Albiter, M. A.; Zaera, F. *Proc. Natl. Acad. Sci. U.S.A.* **2008**, *105*, 15241–15246.
(40) Tao, F.; Grass, M. E.; Zhang, Y.; Butcher, D. R.; Renzas, J. R.; Liu, Z.; Chung, J. Y.; Mun, B. S.; Salmeron, M.; Somorjai, G. A. *Science* **2008**, *322*, 932–934.
(41) Friedrich, H.; Jongh, P. E.; Verkleij, A. J.; Jong, K. P. *Chem. Rev.* **2009**, *109*, 1613–1629.
(42) Tojo, T.; Zhang, Q.; Saito, F. *J. Alloys Compd.* **2007**, *427*, 219–222.
(43) Fana, W.; Zhao, W.; You, L.; Songa, X.; Zhanga, W.; Yua, H.; Sun, S. *J. Solid State Chem.* **2004**, *177*, 4399–4403.
(44) Mahapatra, S.; Ramanan, A. *J. Alloys Compd.* **2005**, *395*, 149–153.
(45) Liu, J.; Li., Y. *Mater. Chem.* **2007**, *17*, 1797–1803.
(46) Liu, J.; Chen, W.; Liu, X.; Zhou, K.; Li, Y. *Nano Res.* **2008**, *1*, 46–55.
(47) Wang, D.; Xie, T.; Li, Y. *Nano Res.* **2009**, *2*, 30–46.
(48) Sheldrick, W. S.; Wachhold, M. *Angew. Chem., Int. Ed.* **1997**, *36*, 206–224.
(49) Demazeau, G. *J. Mater. Chem.* **1999**, *9*, 15–18.
(50) Walton, R. I. *Chem. Soc. Rev.* **2002**, *31*, 230–238.
(51) Nguyen, T. D.; Do, T. O. *Langmuir* **2009**, *25*, 5322–5332.
(52) Nguyen, T. D.; Mrabet, D.; Do, T. O. *J. Phys. Chem. C* **2008**, *112*, 15226–15235.
(53) Kwon, S. G.; Piao, Y.; Park, J.; Angappane, S.; Jo, Y.; Hwang, N. M.; Park, J. G.; Hyeon, T. *J. Am. Chem. Soc.* **2007**, *129*, 12571–12584.
(54) Fana, W.; Zhao, W.; You, L.; Songa, X.; Zhanga, W.; Yua, H.; Sun, S. *J. Solid State Chem.* **2004**, *177*, 4399–4403.
(55) Mialon, G.; Gohin, M.; Gacoin, T.; Boilot, J. P. *ACS Nano* **2008**, *2*, 2505–2512.
(56) Xie, T.; Li, S.; Peng, Q.; Li, Y. *Angew. Chem.* **2009**, *121*, 202–206.
(57) Shevchenko, E. V.; Talapin, D. V.; Schnablegger, H.; Kornowski, A.; Festin, Ö.; Svedlindh, P.; Haase, M.; Weller, H. *J. Am. Chem. Soc.* **2003**, *125*, 9090–9101.
(58) Peng, Z. A.; Peng, X. *J. Am. Chem. Soc.* **2002**, *124*, 3343–3353.
(59) Yin, Y.; Alivisatos, A. P. *Nature* **2004**, *437*, 664–670.
(60) Nguyen, T. D.; Do, T. O. *J. Phys. Chem. C* **2009**, *113*, 11204–11214.

Downloaded by UNIV LAVAL on October 22, 2009 | http://pubs.acs.org
Publication Date (Web): October 6, 2009 | doi: 10.1021/jp907129t

(61) Hughes, M. D.; Xu, Y. J.; Jenkins, P.; McMorn, P.; Landon, P.; Enache, D. I.; Carley, A. F.; Attard, G. A.; Hutchings, G. J.; King, F.; Stitt, E. H.; Johnston, P.; Griffin, K.; Kiely, C. J. *Nature* **2005**, *437*, 1132–1135.

(62) Patel, D.; Andersen, P. J.; Kung, H. H. *J. Catal.* **1990**, *125*, 132–145.

(63) Jia, C. J.; Sun, L. D.; Luo, F.; Jiang, X. C.; Wei, L. H.; Yan, C. H. *Appl. Phys. Lett.* **2004**, *45*, 5305–5307.

(64) Mahapatra, S.; Ramanan, A.*J. Alloys Compd.* **2005**, *395*, 149.

(65) Deng, H.; Yang, S.; Xiao, S.; Gong, H. M.; Wang, Q. Q. *J. Am. Chem. Soc.* **2008**, *130*, 2032.

(66) Moulder, J. F.; Stickle, W. F.; Sobol, P. E.; Bomben, K. D. *Handbook of X-ray Photoelectron Spectroscopy*; Perkin-Elmer Corporation, Physical Electronics Division: Waltham, MA, 1992.

(67) Selvan, R. K.; Gedanken, A.; Anilkumar, P.; Manikandan, G.; Karunakaran, C. *J. Clust. Sci.* **2008**, DOI 10.1007/s10876-008-0229-y.

(68) Mrabet, D.; Zahedi-Niaki, M. H.; Do, T. O. *J. Phys. Chem. C* **2008**, *112*, 7124–7129.

(69) Song, J.; Ren, L.; Yin, C.; Ji, Y.; Wu, Z.; Li, J.; Xiao, F. S. *J. Phys. Chem. C* **2008**, *112*, 8609–8613.

(70) Wang, X.; Li, Y. *Chem. Comm.* **2007**, 2901–2910.

JP907129T

Downloaded by UNIV LAVAL on October 22, 2009 | http://pubs.acs.org
Publication Date (Web): October 6, 2009 | doi: 10.1021/jp907129t

A Novel Approach for Monodisperse Samarium Orthovanadate Nanocrystals: Controlled Synthesis and Characterization

Thanh-Dinh Nguyen,[a] Cao-Thang Dinh,[a] Dinh-Tuyen Nguyen,[b] and Trong-On Do*[a]

Department of Chemical Engineering, Laval University, Quebec G1K 7P4 Canada,[a] and Institute of Chemistry, Vietnamese Academy of Science and Technology (VAST)[b]

To whom correspondence should be addressed. E-mail: Trong-On.Do@gch.ulaval.ca

SUBMITTED TO ***J. Phys. Chem. C*** –July 2009

Supporting Information

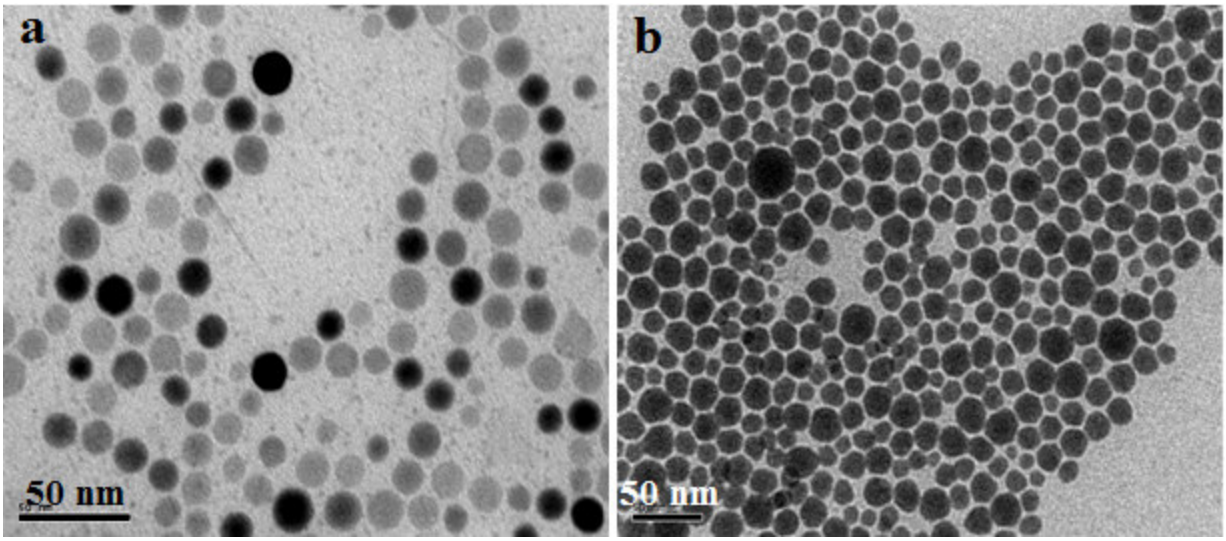

S-Figure 1. TEM images of the $SmVO_4$ nanocrystals synthesized at 180 ^oC for 24 h from a 1:1 toluene solution containing precursors ([$(Sm(OA)_3$] = [$VO_4(TOA)_3$] = 0.065 M) using various surfactants (0.129 M): (a) oleylamine and (b) oleic acid.

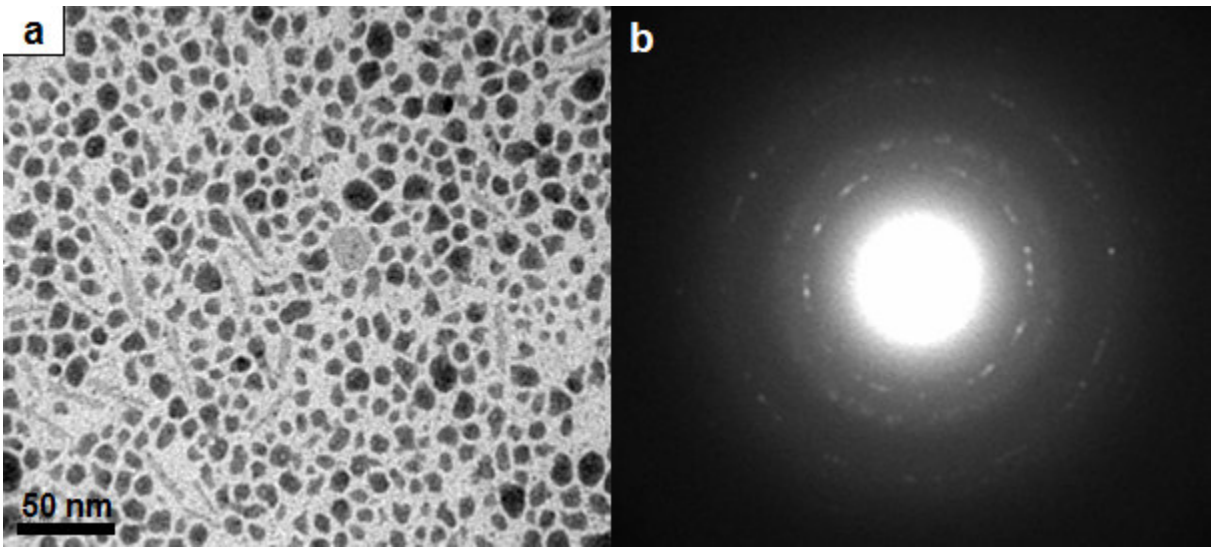

S-Figure 2. TEM image (a) and corresponding SAED pattern (b) of the $SmVO_4$ nanocrystals synthesized from the mixture of $Sm(OA)_3$ and $VO_4(TOA)_3$ complexes in toluene without surfactant at 180 ^oC for 16 h.

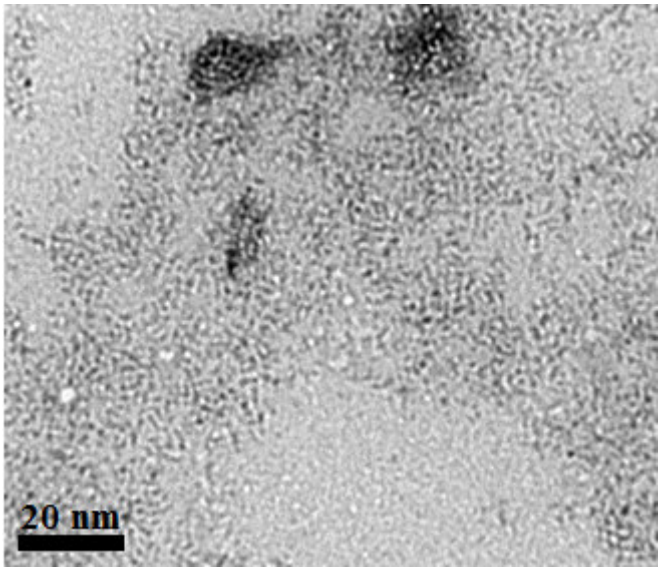

S-Figure 3. TEM image of the $SmVO_4$ gels synthesized at 180 ^{o}C for 16 h using 0.01 M of $Sm(OA)_3$ and $VO_4(TOA)_3$ complexes with Sm:V of 1, and oleylamine:precursor of 4.